Physics – Uspekhi **60** (6) 608 – 620 (2017)

FROM THE CURRENT LITERATURE PACS number: **52.90.+z**

Electrohydrodynamic flow for the active control of gas flows

V Yu Khomich, V A Yamshchikov

DOI: https://doi.org/10.3367/UFNe.2017.01.038047

Contents

Abstract. A new approach to producing powerful electrohydrodynamic flows in a gas environment is discussed, in which a barrier discharge distributed over a dielectric surface is used as an intense ion source. Electric discharge systems for active control of gas flows with a high ($> 15\,\mathrm{l\,s^{-1}}$) volumetric rate are developed and investigated. A highly effective multidischarge actuator system is created to control air flows over aerodynamic surfaces with a significantly higher actuator force and energy characteristics than those in known global analogs.

Keywords: electrohydrodynamic flow, ion beam, barrier discharge, multidischarge actuator

1. Introduction

Electrohydrodynamic (EHD) flows are produced as a result of interaction between a gas discharge plasma and the ambient gas medium. An EHD flow represents the joint motion of gas and charged particles drifting under the action of a strong electric field, and is created by ions transferring their momenta to neutral gas components in collisions [1–6]. This phenomenon also includes the effect historically known under the name 'electric wind', discovered by the English scientist Francis Hauksbee, the Elder [1] at the beginning of the 18th century.

V Yu Khomich, V A Yamshchikov Institute of Problems of Electrophysics, Russian Academy of Sciences,
Dvortsovaya nab. 18, 191186 St. Petersburg, Russian Federation
E-mail: khomich@ras.ru, yamschikov52@mail.ru

Received 9 August 2016, revised 8 September 2016
Uspekhi Fizicheskikh Nauk **187** (6) 653 – 666 (2017)
DOI: https://doi.org/10.3367/UFNr.2017.01.038047
Translated by S D Danilov; edited by A Radzig

Electric wind was traditionally applied in machine tools for electron–ion technologies, in electric filters for cleaning gas media, an in instruments for electric painting and the deposition of coatings on materials [7–9]. In the computer industry, the new technology of computer chip cooling with the aid of electric wind has been applied to intensify heat removal in modern high-performance computer systems [10–13].

Over recent years, increased interest can be seen in research on EHD flows, which stems from the possibility of forming fast gas flows without electromechanical units, such as turbines and fans. A promising atmospheric plasma technology aimed at active control of gas boundary-layer flows on aerodynamic surfaces [6, 14–17] is also related to the EHD interaction between charged and neutral particles. Units creating EHD flows are used for electrical pumping of a gas mixture in electric discharge lasers [18–23].

At present, a pressing problem is the generation of powerful EHD flows and active control of rather extended gas flows with a high volumetric rate. In work on new approaches and tools of flow generation, particular attention is paid to the possibility of efficient control of the air flow distribution profile and velocity, parameter optimization of power supply hardware, and improvement of electrode system design; these topics constitute the subject of this paper.

The electric wind mentioned above is generated on pointed or thin conductors engaged in a corona discharge. The employment of a corona discharge allows relatively large wind velocities (4–5 m $\mathrm{s^{-1}}$) to be reached, but in this case the volumetric rate of gas flow is bounded by 2–3 $\mathrm{l\,s^{-1}}$, because of the smallness of the area where the discharge glows [18, 20, 22, 24, 25]. When multielectrode corona systems are exploited, mutually interfering close discharges weaken each other, and a substantial increase in the resulting flow rate is not

observed. Moreover, the stability of the corona discharge is substantially affected by the ambient gas state [25, 26].

Frequently an EHD flow is formed using a dielectric barrier discharge, which has increased stability relative to the changes in the ambient medium state. In this case, if sufficiently high AC voltage is applied to the electrodes in the form of narrow strips separated by a flat dielectric, a barrier discharge is ignited on one of electrode edges. This discharge induces a gas flow confined to a narrow region (several mm thick) near the surface of the dielectric and also limited in amplitude [6, 16, 17].

In 2003, we proposed a new approach to the generation of powerful EHD flows, based on the interaction of neutral gas with a high-intensity ion flow excited by a barrier discharge distributed over the surface of a dielectric [21]. In that paper, we also proposed an electric setup to generate the gas flow with a high volumetric rate by combining a near-surface high-frequency barrier discharge and external high-voltage electrode system, in which the gas flow is maintained through ion acceleration in a strong electric field and momentum transfer from the ions to gas molecules. In this setup, power supply to the barrier discharge proceeds from one AC source and the current of ions drifting in the external electric field is energized independently from the other high-voltage source, which offers additional options for controling gas flows [20, 27].

A prototype of a high-voltage system with a source of charged particles was the electrode system (frequently called the Dumanchin system), which we utilized earlier in powerful electric-discharge CO_2-lasers to produce initial electrons and subsequently fill the laser discharge gap with electrons through their drift in an electric field [28, 29]. The cathode in this system was made of a metal plate and RK-50 preliminarily stripped RF cable 4 mm in diameter, which was tightly fitted into transverse grooves milled into the working surface of this plate. On applying a high-voltage pulse between the cable wire and the plate, a barrier discharge was ignited on the dielectric parts of the cable, external with respect to the plate, being distributed over the entire working surface of the cathode. The electrons were expelled from the plasma surface of the cathode unit and moved to the anode under the action of the field between the main laser electrodes.

In practice, the so-called Dumanchin electrode system is impenetrable to the gas flow. We therefore proposed a construction of a flat-cylindrical electrode module comprising a plasma ion emitter implemented as a dielectric tube with the barrier discharge ignited on its surface, and an ion collector made of planar metal grid placed over the emitter. A schematic of the plasma emitter design (without the grid) is depicted in Fig. 1. Such a construction does not interfere with the passage of gas flows. Furthermore, the area of charged particle emission can be extended further by adding modules in parallel and increasing through that the volumetric rate of accelerated gas within given limits [27, 30, 31].

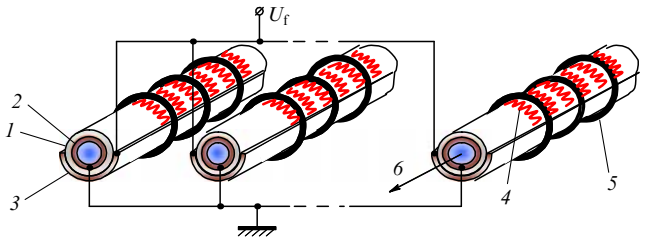

Figure 1. Schematic of a plasma ion emitter: *1* — dielectric tube, *2* — copper tube, *3* — copper gutter-shaped electrode, *4* — barrier discharge, *5* — wire, and *6* — water cooling; U_f is the AC voltage.

2. Theoretical model of electrohydrodynamic flow

EHD interaction represents a rather complex physical process described by a system of equations stemming from two branches of physics, electrostatics and gas hydrodynamics, and taking into account the transport of electric charges [32–34].

The electric potential U satisfies the Poisson equation

$$\nabla^2 U = -\frac{q}{\varepsilon_0}\,, \tag{1}$$

where q is the spatial charge density, and ε_0 is the vacuum permittivity.

The electric potential is also related to the electric field strength

$$\mathbf{E} = -\nabla U\,. \tag{2}$$

The law of charge conservation is written down as

$$\frac{\partial q}{\partial t} + \nabla \mathbf{j} = S_n\,, \tag{3}$$

where S_n are the charge sources and sinks, and $\mathbf{j}$ is the electric current density vector.

The electric current in the zone of charged particle drift is the result of the presence of conductivity (the directed motion of ions in a gas under the action of an electric field), as well as convection (charge transport in a gas flow) and diffusion. Taking this into account, we arrive at the expression

$$\mathbf{j} = \mu_i \mathbf{E} q + \mathbf{V} q - D\nabla q\,, \tag{4}$$

where μ_i is the ion mobility in gas, $\mathbf{V}$ is the gas flow velocity vector, and D is the ion diffusion coefficient. The term describing convection in equation (4) can be ignored, because $\mathbf{V} \ll \mu_i \mathbf{E}$ [32].

In agreement with the electrodynamic equation connecting the electric field and flow in a charged medium, the force $\mathbf{F}_E$ acting on an ion in an electric field with the relative dielectric constant ε, density ρ, and temperature T is expressed as

$$\mathbf{F}_E = q\mathbf{E} - \frac{1}{2} E^2 \nabla\varepsilon + \frac{1}{2} \nabla\left[E^2 \left(\frac{\partial\varepsilon}{\partial\rho}\right)_T \rho\right]. \tag{5}$$

The first term in Eqn (5) is the Coulomb force acting on a free charge in a gas medium, the second and third terms are the dielectrophoretic and electrostrictive forces, respectively.

The hydrodynamical part of the model is described by the Navier–Stokes equations for an incompressible gas [35]. The system of equations consists of the equation of motion

$$\rho \frac{\partial \mathbf{V}}{\partial t} + \rho(\mathbf{V}\nabla)\mathbf{V} = -\nabla p + \mathbf{F} \tag{6}$$

and the continuity equation

$$\nabla \mathbf{V} = 0\,, \tag{7}$$

where ρ is the gas density, p is the pressure in the gas flow, and $\mathbf{F}$ is the vector field of mass forces.

With account for medium viscosity and formula (5), the momentum conservation law takes the form

$$\rho \frac{\partial \mathbf{V}}{\partial t} + \rho(\mathbf{V}\nabla)\mathbf{V} = \mu\nabla^2\mathbf{V} - \nabla p + \mathbf{F}_E\,, \tag{8}$$

where μ is the gaseous medium dynamic viscosity.

The second and third terms on the right-hand side of equation (5) for the electrodynamic force $\mathbf{F}_E$ are important for a phase transition when the fluctuation of permittivity on the liquid–gas interface is large. The third term contributes substantially if the density fluctuations on the interface between the two media are large. In a gas, the variations in permittivity can be disregarded and the main contribution will then came from the Coulomb force. Under these conditions, we get

$$\rho \frac{\partial \mathbf{V}}{\partial t} + \rho(\mathbf{V}\nabla)\mathbf{V} = \mu\nabla^2\mathbf{V} - \nabla p - q\nabla U\,, \tag{9a}$$

$$\nabla\mathbf{V} = 0\,. \tag{9b}$$

The effect of viscosity is routinely disregarded if the boundaries are distant. The system of the above equations represents the mathematical model used by us for analytical computations and numerical simulations of EHD flows.

2.1 Computation of ion current parameters

The barrier discharge distributed over the surface of a dielectric can serve as a source of charged particles with a bulk density in excess of 10^9 cm^{-3} and can be realized in electrode systems resembling the Dumanchin system, with the area exceeding 1000 cm^2 [21, 29]. To theoretically analyze the processes taking place in the gap between the plasma emitter and ion collector, a simplified one-dimensional model was formulated.

It was assumed that the x-axis is directed from the emitter to the collector, implemented as two infinite parallel planes separated by an interelectrode gap of width d. First, the drift of ions with the concentration $n(x, t)$ in the external electric field $E(x, t)$ is considered. From the full system of equations (1)–(9), only equations of electrostatics and charge motion (1)–(4) were taken into account. Then, the system of equations (5)–(9) was used to compute the hydrodynamics of a neutral gas under the action of a flux of charged particles.

If one ignores the diffusion and convection processes in equation (4) and assumes that the charge sources and sinks related to the ionization multiplication of electrons and loss of charged particles are absent, the system with boundary and initial conditions can be written out as the following system of equations:

• equations of continuity

$$\frac{\partial n(x,t)}{\partial t} + \frac{\partial\big(n(x,t)\mu_\mathrm{i}E\big)}{\partial x} = 0\,, \tag{10}$$

• equations of field change under the action of a bulk charge

$$\frac{\partial E}{\partial x} = \frac{n(x,t)e}{\varepsilon_0}\,, \tag{11}$$

• boundary condition at the emitter

$$n(0,t) = \mathrm{const} = n(0)\,, \tag{12}$$

• boundary condition at the collector

$$n(d,0) = 0\,, \tag{13}$$

• and the boundary condition characterizing the distribution of the electric field strength along the gap length for a given potential difference U_0 between the emitter and collector electrodes:

$$\int_0^d E(x,t)\,\mathrm{d}x = U_0\,, \tag{14}$$

where e is the electron charge.

Assuming $E(x, t) = E(x) = E$ and $n(x, t) = n$, we transform continuity equation (10) into the form

$$\frac{\partial n}{\partial t} + \mu_\mathrm{i}E\frac{\partial n}{\partial x} + \mu_\mathrm{i}n\frac{\partial E}{\partial x} = 0\,. \tag{15}$$

From equation (11), we find

$$n = \frac{\varepsilon_0}{e}\frac{\partial E}{\partial x}\,.$$

The solution for the stationary current regime in the gap between the electrodes is $\partial n/\partial t = 0$. Inserting the expression for n in equation (15), we obtain

$$\frac{\varepsilon_0}{e}\,\mu_\mathrm{i}E\frac{\partial^2 E}{\partial x^2} + \frac{\varepsilon_0}{e}\,\mu_\mathrm{i}\,\frac{\partial E}{\partial x}\frac{\partial E}{\partial x} = 0\,. \tag{16}$$

The previous equation can be written down in the form

$$\frac{\partial}{\partial x}\left(\frac{\partial E}{\partial x}\,E\right) = 0\,. \tag{17}$$

For stationary conditions, in the case of a one-dimensional model describing ion drift in the external electric field between the plane-parallel emitter and the ion collector, analytical expressions were obtained for the distribution of electric field strength $E(x)$, ion concentration $n(x)$, and ion current density $j(x)$ along the x-axis aligned with the field [21, 27, 30, 31]. If the ion concentration at the emitter $n(0)$ is sufficiently large to satisfy the condition

$$\delta = \frac{3}{4}\,\frac{\varepsilon_0 E_0}{en(0)d} \ll 1\,,$$

the solutions take the form

$$E(x) = \frac{3}{2}\,E_0\sqrt{\frac{x}{d} + \delta^2}\,, \tag{18}$$

$$n(x) = \frac{3}{4}\,\frac{\varepsilon_0 E_0}{ed}\,\sqrt{\frac{d}{x + d\delta^2}}\,, \tag{19}$$

$$j = \frac{9}{8}\,\mu_\mathrm{i}\varepsilon_0\,\frac{E_0^2}{d}\,(1 - 3\delta^2)\,, \tag{20}$$

where $E_0 = U_0/d$ is the mean electric field strength in the gap between the electrodes.

For the characteristic values of $E_0 = 10$ kV cm^{-1} and $d = 2$ cm, the condition $\delta \ll 1$ is satisfied for $n(0) \gg 10^9$ cm^{-3}. Such concentrations of charged particles are realized in the barrier discharge.

To compare theoretical results with experimental data, one needs the volt–ampere characteristics of ion current $I = jS$ flowing through the interelectrode gap as a function of voltage U_0. The dependence of current I on the voltage U_0 at the collector is described by the expression

$$I = Sj = \frac{9}{8}\,S\mu_\mathrm{i}\varepsilon_0\,\frac{U_0^2}{d^3} \approx S\mu_\mathrm{i}\varepsilon_0\,\frac{U_0^2}{d^3}\,, \tag{21}$$

where S is the effective area of the ion emitter.

2.2 Computation of gas flow velocity

To compute the velocity of EHD flow we make use of the technique presented in Ref. [36]. If we disregard diffusion and convective charge transports in equation (4) because of their smallness against the drift transport, as well as the viscous term in equation (9), then the force due to the action of electric field $E(x)$ on the spatial ion charge $n(x)$ creates the following pressure gradient in gas:

$$\frac{\mathrm{d}p}{\mathrm{d}x} = n(x)eE(x) = \frac{j(x)}{\mu_\mathrm{i}} \,. \tag{22}$$

Taking into account expression (20) for $j(x)$ and the relationship $\delta \ll 1$, we find the pressure due to electric forces near the grid collector:

$$p = \frac{1}{\mu_\mathrm{i}} \int_0^d j(x)\,\mathrm{d}x = \frac{9}{8}\,\varepsilon_0 E_0^2 \,.$$

The quantity p near the grid can also be written in the form $p = \rho V^2$, where ρ is the gas density in the interelectrode gap and V is the gas flow velocity. Equating these expressions, we get

$$V = \sqrt{\frac{9}{8}\,\frac{\varepsilon_0}{\rho}}\,E_0 \approx \sqrt{\frac{\varepsilon_0}{\rho}}\,E_0 \,. \tag{23}$$

Taking $\varepsilon_0 = 8.85 \times 10^{-12}$ F m^{-1}, and $\rho = 1.29$ kg m^{-3} for air at the temperature of 0 °C [37], we find

$$V\ [\mathrm{m\ c^{-1}}] \approx 0.28 E_0\ [\mathrm{kV\ cm^{-1}}] \,. \tag{24}$$

The stationary model considered above allows us to analyze basic electrophysical characteristics and relationships among them for the EHD flow in the case of a planar electrode configuration.

3. Experimental studies of electrohydrodynamic flows

3.1 Experimental setup

In experimental studies of EHD flow, the setup presented in Fig. 2 has been employed. It uses a plasma ion emitter with a high-frequency barrier discharge distributed over the dielectric surface. The construction of the plasma emitter consists of a dielectric tube (*1*) (made of Al_2O_3 ceramics) 10 mm in diameter and 30 cm in length. A copper tube (*2*) serving an internal electrode is placed inside tube *1*. The external electrode is copper gutter (*3*) 20 cm in length. A copper wire 0.5 mm in diameter is wound around the tube and gutter with a step of 5 mm. The latter was selected experimentally judging by the uniformity of discharge glowing on the tube surface.

The voltage from a high-voltage generator (*5*) of high-frequency pulses was applied to the external electrodes of the plasma emitter, and the internal electrode was connected to ground through the current shunt r_s. In this case, a plasma layer of barrier discharge was generated on the external surface of the dielectric tube. Heat released during the functioning of the plasma emitter was removed by water (*6*) flowing through tube *2*. The number of tubes connected in parallel to the high-voltage generator of high-frequency pulses was varied from one to three (see Fig. 1).

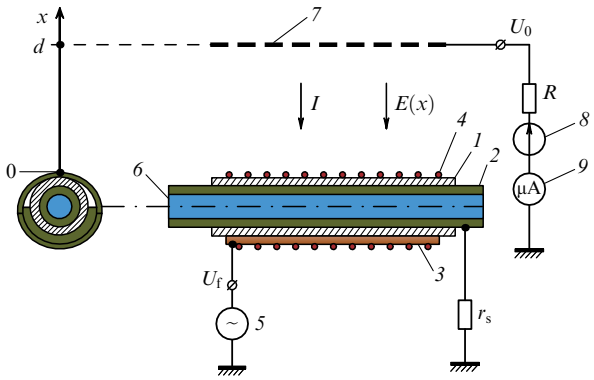

Figure 2. Schematic of experimental setup: *1* — dielectric tube made from Al_2O_3 ceramics, *2* — copper tube (inner electrode), *3* — copper gutter-shaped electrode (outer electrode), *4* — copper wire, *5* — high-voltage generator of high-frequency pulses, *6* — running water, *7* — metal grid, *8* — high-voltage DC source, and *9* — microammeter.

A metal grid (*7*) with transparency $T \approx 0.7$ was installed above the plasma emitters; it served as the ion collector. The distance d from the collector to the emitter was varied. Through the limiting resistor $R = 110$ kΩ, a DC voltage $U_0 = 0-22$ kV of positive polarity was applied to the grid from the high-voltage power supply (*8*). Under the action of external field $E(x)$, the electrons were expelled from the barrier discharge plasma. As a result of the reaction of three-body electron attachment to oxygen molecules, negative ions were formed [38], which moved towards the grid. The accompanying electric current I was registered by a microammeter (*9*).

The setup measuring the characteristics of the EHD flow consisted of a low-induction ohmic shunt with the resistance $r_\mathrm{s} = 0.3$ Ω, a high-voltage Tektronix P6015A probe, and a two-channel LeCroy WaveRunner 6051A oscilloscope. The velocity of air flow was measured by a digital ATT-1004 thermoanemometer.

In the course of experiments carried out in air under room temperature conditions, the influence of the parameters of the high-voltage generator of high-frequency pulses, the electrode system, and the amplitude and polarity of high voltage at the grid on the electric discharge and gasdynamic characteristics of the EHD flow were explored for two regimes of plasma emitter power supply from specially developed voltage generators (*5*). The first one is the G-1 generator of sinusoidal voltage with an amplitude up to ±7 kV and frequency of 30 kHz, and the second one is the G-2 generator of rectangular pulses with a duration of 7 μs and amplitude up to 12 kV and tunable frequency up to 25 kHz. The description and design principle of a similar fully solid-state generator are presented in Refs [39–45].

3.2 Electrohydrodynamic flow for plasma emitters powered by sinusoidal voltage

Oscillograms of the voltage and current from the G-1 generator powering the plasma emitter showed that a series of spontaneous peaks with amplitudes up to 10 mA was present in addition to the reactive component in the oscillogram of current passing through r_s. They appeared at the stages when positive and negative voltage halfwaves were growing, which is related to a multistreamer mechanism of barrier discharge development [44].

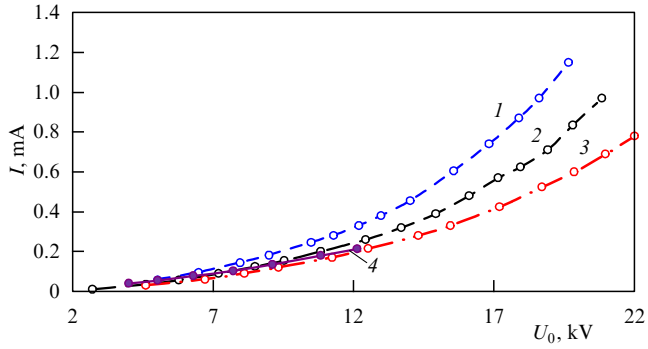

Figure 3. Experimental dependences of ion current I flowing from the emitter to the grid as a function of the grid voltage U_0 for various distances between the emitter and collector: $d = 17$ mm (curves *1* and *4*), $d = 20$ mm (curve *2*), and $d = 22$ mm (curve *3*) for two tubes of the plasma emitter.

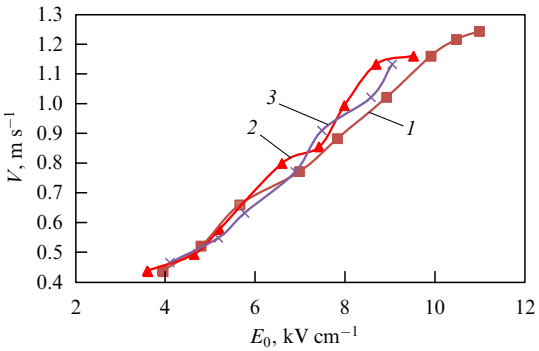

Figure 4. Experimental dependences of EHD flow velocity V on the field strength $E_0 = U_0/d$ in the gap between the emitter and collector for the various distances between them: $d = 18$ mm (curve *1*), $d = 20$ mm (curve *2*), and $d = 22$ mm (curve *3*).

Experimental dependences of ion current I on grid voltage U_0 with positive (curves *1–3*) and negative (curve *4*) polarities of the grid are shown in Fig. 3 for the plasma emitter driven by voltage with amplitude $U_f = \pm 4.5$ kV and frequency $f = 30$ kHz for distances between the emitter and collector $d = 17$, 20, and 22 mm. These dependences agree satisfactorily with formula (21) in the range of U_0 from 4 to 20 kV.

Figure 4 plots the experimental dependences of the induced velocity V of the EHD flow in air on the field strength E_0 at $d = 18$, 20, and 22 mm ($U_f = \pm 5$ kV and $f = 30$ kHz). These dependences are well fitted by a single straight line, which agrees with formulas (23) and (24); however, the slope $V/E_0 \approx 0.11$ m s^{-1} kV^{-1} cm of these experimental dependences is nearly one third the computed value of 0.28 m s^{-1} kV^{-1} cm [see formula (24)].

Since the velocity of EHD flow is proportional to the electric field strength in the interelectrode gap, the maximum flow velocity V_{max} must be bounded by the maximum amplitude E_0^{max} of electric field, which is determined by the breakdown field strength E_{br} for the gap between the emitter and collector.

In a weakly ionized air gap with a nonuniform electric field, one has $E_{br} = 10-15$ kV cm^{-1}. According to Eqn (18), the field $E(x)$ in our conditions reaches its maximum $E(d)$ at the collector. Setting $E(d) = E_{br}$, we get an estimate of electric strength: $E_0^{max} = 7-10$ kV cm^{-1}. When $d = 1.8$ cm, $U_f = 5$ kV, and $f = 30$ kHz, the breakdown occurred for U_0 exceeding 20 kV, which corresponds to $E_0^{max} \approx 10$ kV cm^{-1} and $V_{max} \approx 1.6$ m s^{-1}.

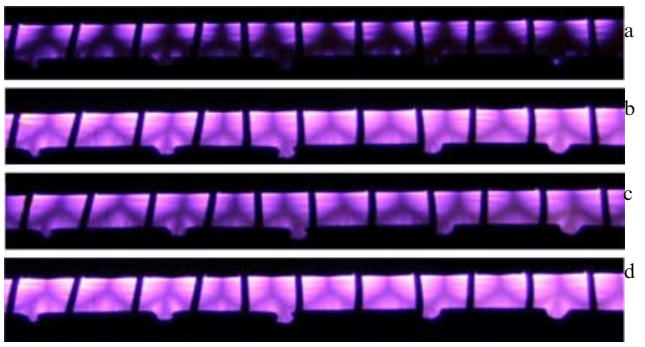

Figure 5. A photograph of barrier discharge glowing on the surface of a plasma emitter for (a) $U_f = 6$ kV and $f = 20$ kHz, (b) $U_f = 10$ kV and $f = 20$ kHz, (c) $U_f = 10$ kV and $f = 10$ kHz, and (d) $U_f = 10$ kV and $f = 25$ kHz.

We see that the above-outlined theoretical model not only illustrates a qualitative shape of volt–ampere and velocity dependences of EHD flow, but also offers simplified analytical expressions for quantitative estimates.

3.3 Influence of magnitude and frequency of voltage powering a plasma emitter on the air flow

The influence of amplitude and frequency of voltage applied to a plasma emitter from the G-2 generator of rectangular pulses has been explored. Oscillograms of voltage and current driving a plasma ion emitter showed that the barrier discharge current was present at the stages when the voltage was either increasing or decreasing [23, 31].

Figure 5 presents photographs of glowing barrier discharge on the surface of dielectric tubes for different values of amplitude U_f and frequency f of the power supply voltage applied to the plasma emitter. The photographs indicate that the higher U_f and f, the larger the surface covered by the discharge plasma, and, hence, the larger the effective area S of ion emission. It has been found experimentally that the ion current increases proportionally to the bias voltage squared on the grid, just as when the plasma emitter was connected to G-1. The current also increased with an increase in U_f and f, which stems from the related increase in the area covered by plasma ($I = jS$) on the surface of a ceramic tube.

Figure 6 demonstrates the experimental dependences of the air flow velocity on the grid voltage for different values of amplitudes and frequencies of the voltage applied to the plasma emitter. Just as in the case when the emitter was powered by G-1, V is directly proportional to U_0. The flow velocity also increased with U_f and f, but up to a certain limit, which indicated that the emitter surface is fully covered with plasma.

Obviously, the discrepancy between the results of the computations described above and experiments is related to approximations taken for the one-dimensional model of EHD flow in a plane-parallel electrode system. In order to learn about the influence of the actual configuration of the setup where the flow is formed, numerical simulations taking into account the peculiarities of the cylindrical construction of the plasma emitter and the planar grid collector are needed.

3.4 Computer modeling of electrohydrodynamic flow

With the aim to determine the limiting parameters of EHD flow and to optimize its spatial profile, a numerical model was developed and used in simulating the EHD flow. The results

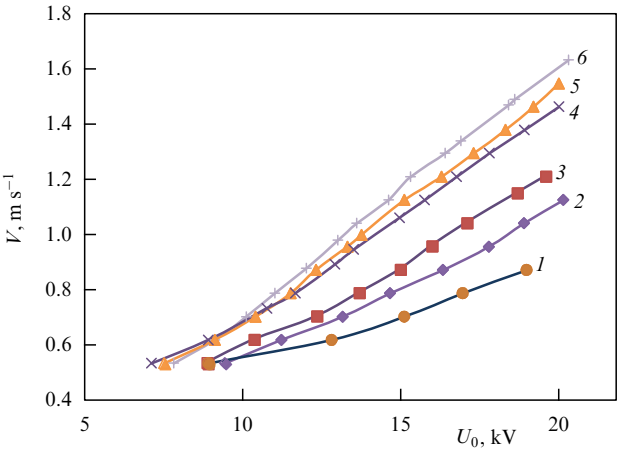

Figure 6. Experimental dependences of the air flow velocity V on the grid voltage U_0 for: $U_f = 6$ kV and $f = 10$ kHz (curve *1*), $U_f = 10$ kV and $f = 10$ kHz (curve *2*), $U_f = 6$ kV and $f = 20$ kHz (curve *3*), $U_f = 10$ kV and $f = 15$ kHz (curve *4*), $U_f = 10$ kV and $f = 20$ kHz (curve *5*), and $U_f = 10$ kV and $f = 25$ kHz (curve *6*).

of modeling the flux of charged and neutral particles emitted in air by the discharge plasma on the surface of a dielectric tube and moving in an external electric field towards the grid are reported in Refs [46–52].

Computer modeling relied on the system of equations (1)–(9) describing the dynamics of ion interaction with neutral gas in an electric field. The following assumptions were adopted for the numerical model:

• the plasma emitter had the shape of a cylinder with a constant charge uniformly distributed over its surface;

• the thickness of the plasma layer at the emitter is negligibly small compared to the cylinder radius;

• only particles of one sign were taken into account.

The geometry of the spatial domain where the EHD flow was simulated corresponds to that of the experimental setup. The coordinate system and the range of computed values are shown in Fig. 7. The ions emitted from the plasma and neutral particles accelerated by them move toward the grid collector under the action of voltage U_0 applied to it. A two-dimensional flow is considered in the transverse plane with respect to the electrodes subject to the following boundary conditions: the constant ion concentration $n(0) \approx 10^{10}$ cm^{-3} on the surface of cylindrical plasma emitter with a radius of 5 mm, the constant voltage across the grid $U_0 = 20$ kV, and a zero potential at the model boundaries. For the hydrodynamic part of the model, the surfaces of grid wires, cylindrical ion emitter, and collector frame were treated as impermeable, without slip at the boundary. The right boundary was placed 80 mm from the grid, which corresponds to the position of the velocity gauge. The main parameters used in numerical modeling are collected in Table 1.

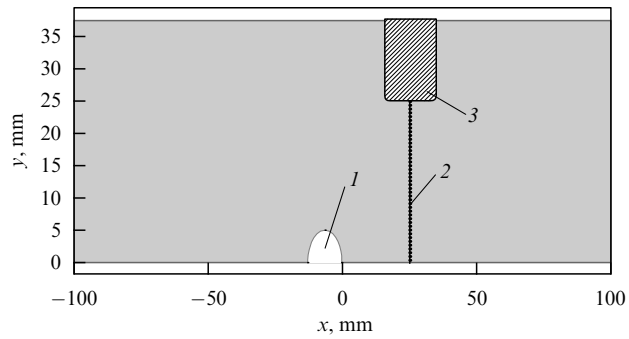

Figure 7. Geometry of the simulated domain: *1* — cylindrical plasma emitter, *2* — grid of the ion collector, and *3* — collector frame.

Table 1. Main parameters used in numerical simulations.

Parameter	Value
Relative permittivity of air, ε	1
Charge diffusion coefficient, D	5.3×10^{-5} m^2 s^{-1}
Ion mobility coefficient, μ_i	1.8×10^{-4} m^2 (V s)$^{-1}$
Air density at 15 °C, ρ	1.23 kg m^{-3}
Air dynamic viscosity, μ	1.8×10^{-5} Pa s
Bulk charge density at the emitter, q_0	10^{-3} C m^{-3}
Distance between the emitter and collector, d	20 mm

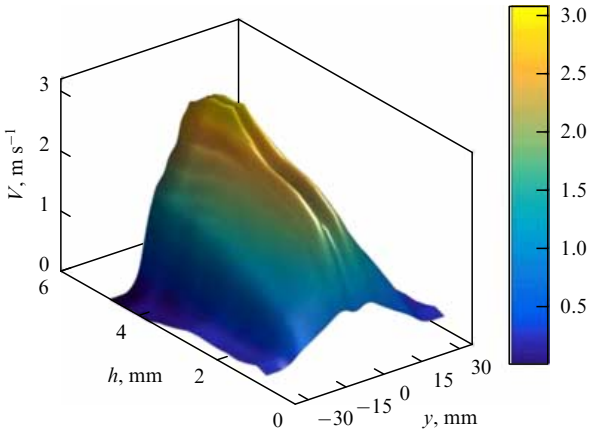

Figure 8. Spatial profile of flow velocity V along the coordinate y as a function of grid pitch h.

The results of computations indicate that the grid electrode greatly impedes the gas motion. It was revealed that flow velocity increases as the grid is made more transparent, which called for optimization in the transparency parameter T of the collector wire grid. For a given wire diameter of 0.5 mm, the value of T was defined by the grid cell size h.

The spatial profile of velocity V distribution along the coordinate y as a function of the grid pitch at the model right boundary, given in Fig. 8, demonstrates the increase in V with T. In simulations, the velocity reaches a maximum value of 3 m s^{-1} at the collector with the geometric grid transparency of 0.83 and the cell pitch of 3 mm. However, as follows from computations, a further increase in T leads to an increase in the electric field strength to 35 kV cm^{-1} on the surfaces of wires composing the grid. This is the result of strong inhomogeneity of the field near the wires and can be the cause of electric breakdown.

3.5 Comparison of experimental and simulated data

To check that the constructed model works correctly and to get a more complete picture of the elapsing processes, some additional comparisons between experimental and computational results have been performed.

The experiments were carried out in atmospheric air under the following conditions: the DC voltage $U_0 = 20$ kV of positive polarity at the grid, the pulses of voltage driving

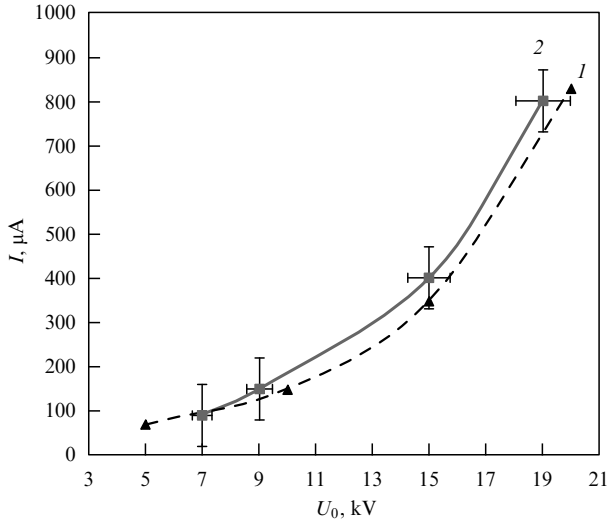

Figure 9. Volt–ampere characteristics of ion current in air: the results of computations (curve *1*) and experiment (curve *2*).

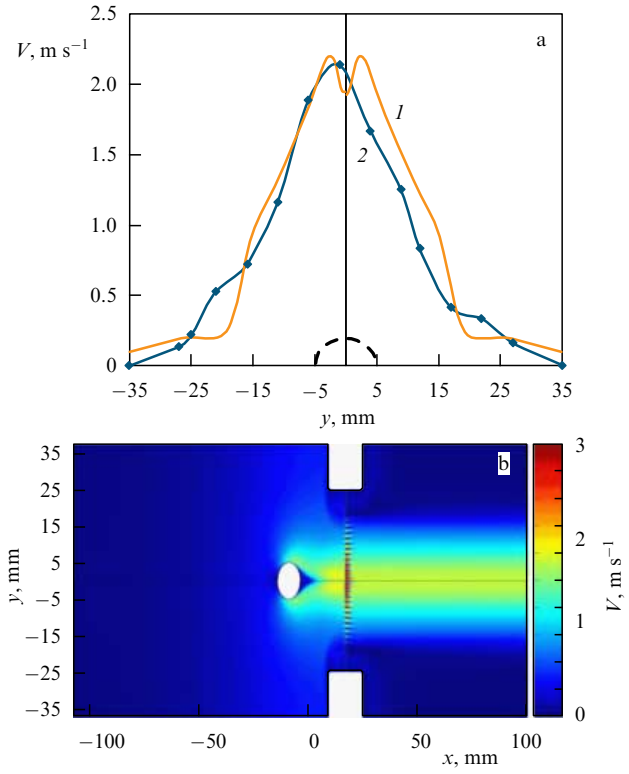

Figure 10. (a) Computed (curve *1*) and experimental (curve *2*) velocity profiles of air flow above a single tube of a plasma emitter in the cross section. The dashed line shows the tube profile. (b) The computed distribution of flow velocity in the plane transverse to the electrodes with one plasma emitter.

the plasma emitter were of a rectangular shape with a duration of 7 μs and amplitude $U_f = 11$ kV at a frequency of 10 kHz, the distance between the plasma emitter and the grid was $d = 20$ mm, and the distance from the grid to the velocity gauge was equal to 50 mm. A brass grid with transparency $T = 0.7$ was used as the collector electrode, at which, as follows from Fig. 9, the simulated and experimental volt–ampere characteristics of ion current in air correlate well with each other.

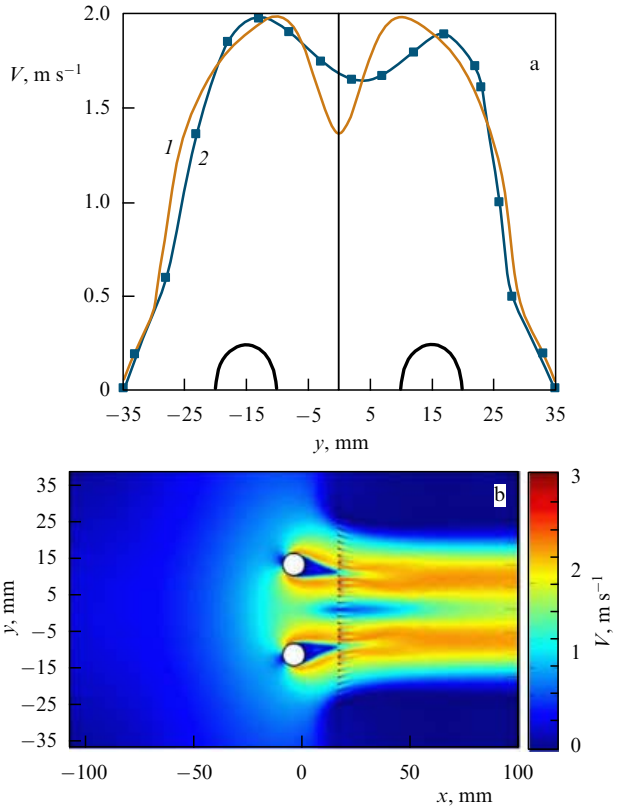

Figure 11. (a) Computed (curve *1*) and experimental (curve *2*) transverse velocity profiles of air flow above two tubes of a plasma emitter (the axes of the tubes shown at the bottom of the plot were at $y = \pm 15$ mm). (b) Computed distribution of flow velocity in the plane transverse to the electrodes with two plasma emitters.

The experimental and computed velocity profiles of the flow above one single tube of a plasma emitter are shown in Fig. 10a in the section perpendicular to the electrodes at a distance of 50 mm from the grid, and the latitudinal distribution of the EHD flow velocity amplitude in the plane perpendicular to the electrodes is given in Fig. 10b, with the maximum velocity exceeding 2 m s^{-1}. Noteworthy is the good agreement between experimental and computational data.

To verify the assumption that the gas flow rate might be scaled if the number of plasma emitters is increased, placing them parallel to each other at the distance l, modeling of the EHD flow has been performed for an electrode system comprising two plasma emitters. The respective velocity profiles of EHD flow in air are illustrated in Fig. 11.

The gas flux is computed as

$$W = L \int_{Y_1}^{Y_2} V(y)\, \mathrm{d}y\,,$$

where Y_1 and Y_2 are the coordinates at which $V = 0$, and L is the length of the plasma emitter. For the case of one and two tubes, the gas fluxes are $W_1 \approx 8$ l s^{-1} and $W_2 \approx 15$ l s^{-1}, respectively. The increase in the width of the EHD flow velocity profile, proportional to the number of plasma emitters, implies an increase in the gas flow rate for preserved maximum flow velocity.

Based on the velocity profile obtained for two cylindrical plasma emitters 10 mm in diameter, one can conclude that there is an optimum distance $l = 20-25$ mm between the two

neighboring emitters, for which the dip in the velocity profile in the center of the flow is at a level of 0.2 from the maximum.

Thus, the results of numerical simulations of EHD flow in a system of cylindrical plasma emitters and a planar grid ion collector agree well with the experimental data, which confirms the applicability of the model developed to simulate and optimize the parameters of EHD systems.

4. Electric discharge laser unit of gas mixture pumping with an electrohydrodynamic flow

In pulse-periodic electric discharge lasers, high-speed gas flows are traditionally formed with the help of fans of various types. Owing to the excitation of acoustic oscillations, gas self-circulation is possible, but it bears a well pronounced resonance character related to the excitation of intrinsic frequencies of the acoustic resonator [53]. An alternative to such pumping systems is offered by electric systems, the functioning of which relies on the effect of electric wind generated by corona discharge.

Research on systems of electric pumping in electric discharge gas lasers is attracts a great deal of attention, because such systems are free of moving parts; hence, there are no related failures due to a rotor wearing out or thermal and mechanical fatigue of fans [18–23]. Such systems are absolutely noise-free, do not create vibrations, and are also sufficiently simple and compact. Furthermore, they provide vacuum purity, which is especially important when pumping aggressive gaseous media.

However, as mentioned in the Introduction, there is a fundamental limitation to the gas flow rate — less than $3\,\mathrm{l\,s^{-1}}$, which comes from too small an area where discharge is glowing. This is insufficient for utilizing the corona discharge in powerful lasers [21, 23]. It is therefore of interest to consider applying the approach presented above, with schemes of EHD flow formation similar to those presented in Figs 1 and 2, to gas mixture pumping in powerful gas discharge lasers.

The most important factor influencing the maximum frequency of pulse repetition in electric discharge lasers is the velocity V_d of working gaseous medium in the laser discharge section. In turn, this velocity is defined by the volumetric rate of gas flow maintained by the pumping system:

$$W = V_\mathrm{d} S_\mathrm{d} = V_\mathrm{d} h l\,,$$

where S_d is the area of the flux in the discharge gap, h is the distance between the electrodes, and l is the discharge length.

Let us estimate the volumetric rate of gas flow and its velocity in the pumping contour for the CL-5000 excimer laser mass produced in Russia [23, 54]. When using excimer mixtures, the coefficient K of gas renewal through the discharge gap, i.e.

$$K = \frac{V_\mathrm{d}}{wf}\,,$$

where w is the discharge width, and f is the pulse repetition rate, should not be less than 4.

The CL-5000 laser possesses the following parameters: $h = 1.2$ cm, $l = 25$ cm, $w \approx 0.3$ cm, $S_\mathrm{d} = 30$ cm^2, and the maximum frequency $f = 300$ Hz [32, 54, 55]. Hence, it follows that the volumetric rate of gas flow $W \geqslant 11\,\mathrm{l\,s^{-1}}$.

Figure 12. Photograph of a unit for gas mixture pumping.

Based on the results of experiments and numerical simulations, it was found that, taking into account gasdynamical losses in the gas mixture pumping contour, one needs no fewer than three tubes similar to those considered above to obtain an EHD flow with the parameters required in the pumping unit.

Figure 12 displays a photograph of the new unit pumping gaseous media of electric discharge lasers, with three tube ion emitters made of metal-ceramic materials. The relatively compact dimensions of the unit allow it to be incorporated in the discharge chamber unit of the CL-5000 laser in place of a fan propeller. Measurements of the volumetric rate of EHD flow in the pumping contour have shown that, if the discharge chamber is filled with air at atmospheric pressure, the unit maintains a flux with $W \geqslant 15\ \mathrm{l\ s^{-1}}$. This is sufficient for pumping a typical mixture in an ArF laser, if it operates at the maximum pulse repetition rate [23].

5. Multidischarge actuator system for an electrohydrodynamic flow

The application of plasma technologies to an active control of aerodynamic flows is considered today as one of most promising areas in aviation science and technology. These include technologies relying on the interaction of discharge plasma ions with the gaseous medium, which generates an EHD flow [16, 17, 26, 31, 46]. Units forming the EHD flow are plasma actuators, which are exploited to exert an effective force on the boundary layer on aerodynamic surfaces. In this case, the gas discharge with a dielectric barrier is created on the surface of a dielectric plate in the gap formed by thin (several dozen micrometers) strips of bare and insulated electrodes arranged on opposite sides of this plate, to which a high AC voltage is applied.

The main advantages of plasma actuators include the absence of moving parts, the possibility of electronic control, a high operating speed, the simplicity of construction and the capacity to adjust it to the shape of aerodynamic surfaces, the stability of barrier discharge to changes in atmospheric pressure and humidity, small energy consumption, and low weight. The drawback of plasma actuators is their limited applicability to air flows with Reynolds numbers less than 10^6 [56].

The fundamental problem consists in strengthening the bulk force exerted on a gas flow with the help of plasma

actuators, which can create a continuous unidirectional air flow on sufficiently extended surfaces with a high efficiency. One of the main ways to increase the induced air flow lies in extending the area of the plasma surface by using a set of discharge gaps located on this surface [57, 58]. Such setups can be called multidischarge actuator systems.

New effects come into play in multidischarge actuators; they are not characteristic of actuators with one discharge gap and arise because of the mutual influence of neighboring electrodes as the distance between them decreases, which limits the applicability of multidischarge actuators [59].

One serious problem related to using multidischarge actuators is that the discharge can be ignited on both (active and passive) edges of a bare electrode strip. As a result, a counterflow is generated, weakening the net effect. To suppress the action of the counterflow, various solutions have been proposed which take advantages of screening electrodes [60] or insulated internal electrodes under a floating potential [61]; a high-voltage electrode made of thin wire and alternating sequence of high-voltage and grounded electrodes [62], and schemes with bipolar type electrodes [63].

To solve the problem mentioned, Ref. [64] put forward the idea of using a multidischarge actuator system based on an improved three-electrode scheme with a screening electrode, in which the role of accelerating electrode is played by a continuous equipotential wing surface. In such a scheme, the negative interference of neighboring actuator electrodes can be reduced to a considerable degree. Furthermore, the scheme proposed helps to essentially miniaturize the plasma actuator systems, which can be a decisive factor if it is applied to a sufficiently thin boundary layer, for example, in the vicinity of a wing leading edge [65].

To increase the energy efficiency of such a scheme of multidischarge actuator systems, optimization was needed of its geometric and physical parameters. We consider below the results of experimental research and computations on the characteristics of air flow induced by barrier discharge and the efficiency of the multidischarge actuator system similar to the one proposed in Ref. [65]; we also compare its parameters with those of the so-called classical electrode system [57, 58].

5.1 Experimental setup to explore plasma actuators

To explore plasma actuators, an experimental setup described in Ref. [66] was designed and built, consisting of the actuator power supply system based on a specially developed high-voltage generator of nanosecond pulses with voltage up to 16 kV, a repetition rate up to 15 kHz, and a mean supply power of 2 kW, and an automated measuring complex to control the parameters of the setup. Depending on the generator scheme, the form of the output voltage can be rectangular, sawtooth, or sinusoidal. The experimental setup allows simultaneous registration of the output generator parameters, and the currents and voltages of barrier discharge, together with spatial scanning of the velocity characteristics of the EHD flow induced near the actuator surface. A spatial resolution of 0.5 mm and accuracy of flow velocity measurements up to 0.1 m s^{-1} were achieved.

The two models of multidischarge actuators explored by us with improved and classical electrode systems are referred to as I and II, respectively. They were prepared by the technology of multilayer printed circuit boards with a base of glass textolite and a copper layer 18 μm in thickness. Their schematics are shown in Fig. 13. As can be seen from Fig. 13c, the classical model (II) lacks a continuous electrode, and the role of accelerating electrodes is taken by electrodes *4*, which, in contrast to the accelerating electrodes of model I, are fully insulated from electrodes *3*.

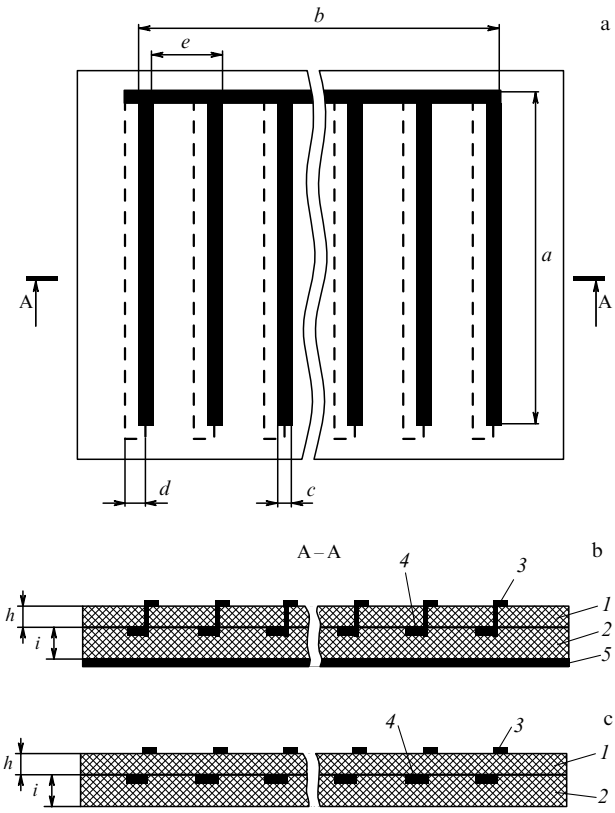

Figure 13. Schematic of multidischarge actuator systems. (a) The top view for models I and II: *a* is the width of the active domain, *b* is the length of the active domain, *c* is the width of the outer active electrode, *d* is the width of insulated screening or accelerating electrodes, *e* is the electrode step. (b) Side view for model I: *1* — the outer dielectric layer, *2* — inner dielectric layer, *3* — outer active electrode, *4* — insulated screening electrode, and *5* — continuous accelerating electrode; *h* is the thickness of the outer dielectric layer; *i* is the thickness of the inner dielectric layer. (c) Side view for model II: *1* — outer dielectric layer, *2* — inner dielectric layer, *3* — outer active electrode, and *4* — insulated accelerating electrode.

Table 2. Geometrical parameters of multidischarge actuator systems.*

Model	*a*, mm	*b*, mm	*c*, mm	*d*, mm	*e*, mm	*h*, mm	*i*, mm
I	245	239.5	1	0.5	7	0.3	0.7
II	115	100	2	2.5	12	0.5	0.5

* See Fig. 13.

The basic parameters of both multidischarge actuator models are given in Table 2.

A photograph of the plate of a multidischarge actuator system with barrier discharge on the surface is given in Fig. 14 for model I. Electrodes *4* (Fig. 13b) screen the adjacent edges of the outer active electrodes *3* with respect to a continuous electrode *5*. When voltage is applied to electrodes *3* and *5*, the electric field on the left edges of electrode *3* turns out to be insufficient for the discharge to be ignited, so the discharge glows only on the right edges of electrode *3*, inducing in this way a unidirectional EHD flow.

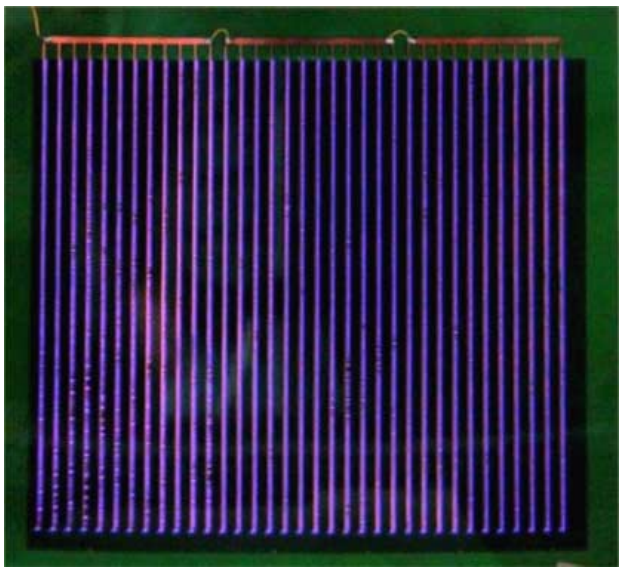

Figure 14. Photograph of the multidischarge actuator system plate with barrier discharge on the surface.

5.2 Methods for determining the plasma actuator power consumption

According to Refs [66, 67], the power consumption by a plasma actuator can be evaluated as

$$P = fU_{\mathrm{d}}(U_{\mathrm{m}} - U_{\mathrm{d}})(C_{\mathrm{d}} - C_0)\,,$$

where U_{d} is the ignition voltage of the barrier discharge, U_{m} is the power supply voltage amplitude, C_{d} is the system capacitance in discharge processes, C_0 is the self-capacitance of the actuator defined by its construction, and f is the voltage frequency.

If the power supplied by the high-voltage generator is raised, the actuator gets heated. Its surface temperature was diagnosed by the Center 350 infrared pyrometer. The limiting temperature for a dielectric made of glass textolite is the vitrification temperature of the binding epoxy resin, about 110 °C, on exceeding which the printed plate may fail. On the other hand, the actuator breakdown voltage is related to the maximum electric field strength for the glass textolite, which is 16.8 kV mm^{-1}. Both factors should be taken into account when selecting the admissible domain of variability for the parameters U_{m}, f, and P of multidischarge plasma actuator power supply.

The energy consumed within a time interval $t_2 - t_1$ is defined as

$$E = \int_{t_1}^{t_2} U(t)I(t)\,\mathrm{d}t = \int_{Q_1}^{Q_2} U\,\mathrm{d}Q\,,$$

where $U(t)$ and $I(t)$ are the voltage and current in the actuator measured by oscillograms, and Q is the charge carried during this time interval.

Part of this energy is released in the discharge, heating the gas, another part is due to losses in the dielectric, a third part is the energy of periodically varying electric and magnetic fields, whereas the still remaining part is transferred to the kinetic energy of the EHD flow.

Computation of the power supply for multidischarge actuator systems was carried out with the help of volt–coulomb characteristics [66, 68–70]. According to this method, first the charge $Q(t)$ carried from the source to the actuator for the time t was computed. In the course of experiments, for each model the oscillograms of the current $I_{\mathrm{a}}(t)$ and voltage $U_{\mathrm{a}}(t)$ at the electrodes of the multidischarge actuator system were obtained as a function of time for various values of U_{m} and f. From the current oscillograms, the charge carried from the electrode unit length was computed:

$$Q(t) = \frac{1}{L_{\mathrm{a}}}\int_{t_1}^{t_2} I(t)\,\mathrm{d}t\,,$$

where L_{a} is the net length of the actuator electrodes.

Based on the measured and computed quantities, the dependences of the voltage $U_{\mathrm{a}}(Q_{\mathrm{a}})$ across the actuator as a function of charge Q_{a} for the full period of voltage variation were constructed. These dependences represent closed curves, for which the areas under the curves were computed:

$$E = \oint U(Q)\,\mathrm{d}Q\,.$$

The last quantity equals the energy scattered in the plasma actuator for one period of voltage oscillations.

The power consumed by the plasma actuator is computed as

$$P_{UQ} = Ef\,.$$

To check the correctness of the procedure applied to determine the power consumed, the method of power measurement from Ref. [65] was also employed. For this, the output current (I_{i}) and voltage (U_{i}) of an idle running generator were measured, then the load was attached and the current (I_{n}) and voltage (U_{n}) of the power supply were measured once again. Based on the measurement results, we computed the power consumption without the load $(P_{\mathrm{i}} = I_{\mathrm{i}}U_{\mathrm{i}})$ and with the load $(P_{\mathrm{n}} = I_{\mathrm{n}}U_{\mathrm{n}})$, and also the specific power consumed by the actuator:

$$P_{UI} = \frac{P_{\mathrm{n}} - P_{\mathrm{i}}}{L_{\mathrm{a}}}\,.$$

An example of the results of measurements and computations is given in Table 3. It should be mentioned that methods based on volt–coulomb and volt–ampere characteristics agree sufficiently well, which indicates that the measurements are reliable and that the simpler volt–ampere method of Ref. [65] can be safely employed.

5.3 Characteristics of electrohydrodynamic flow velocity and efficiency of multidischarge actuator systems

When optimizing parameters of both models of multidischarge actuator systems, it was supposed that their

Table 3. Power consumption of model I for $U_{\mathrm{m}} = 4$ kV.

f, kHz	P_{n}, W	P_{i}, W	$P_{\mathrm{n}} - P_{\mathrm{i}}$, W	P_{UI}, W m^{-1}	P_{UQ}, W m^{-1}
4	80	11	69	9	10
6	119	19	100	13	13
8	168	25	143	19	19
10	221	31	190	25	23
12	264	37	227	30	28
14	323	48	275	36	31
16	377	55	322	43	36
18	421	60	361	48	42

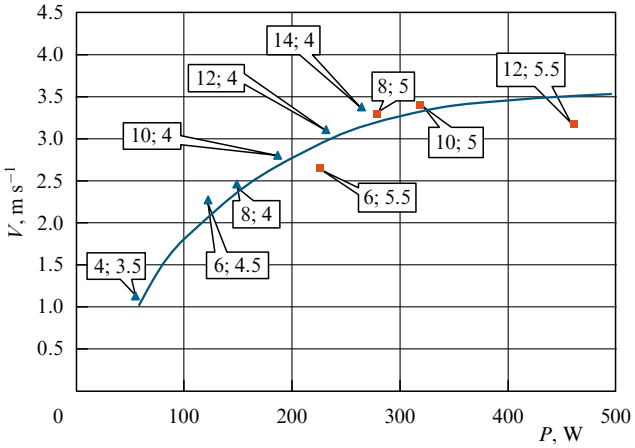

Figure 15. Experimental dependence of the maximum velocity V of induced flow on the power P for various values of f [kHz] and U_m [kV], given as pairs of numbers (in boxes) in the (P, V) plane.

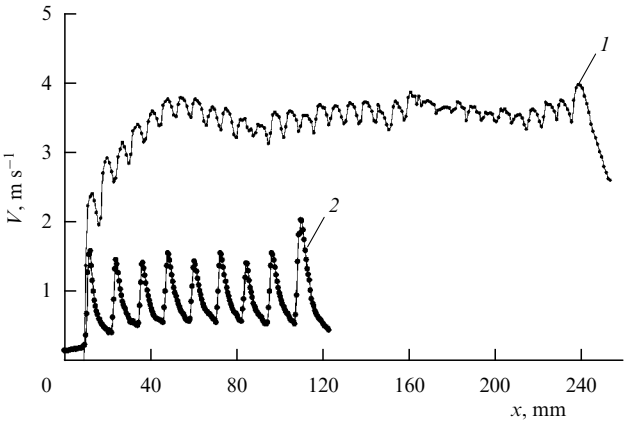

Figure 16. Longitudinal profiles of induced air flow velocity $V(x)$ at a height of 0.5 mm from the surface for the pulse frequency 12 kHz and power supply voltage 4.8 kV for model I (*1*) and model II (*2*).

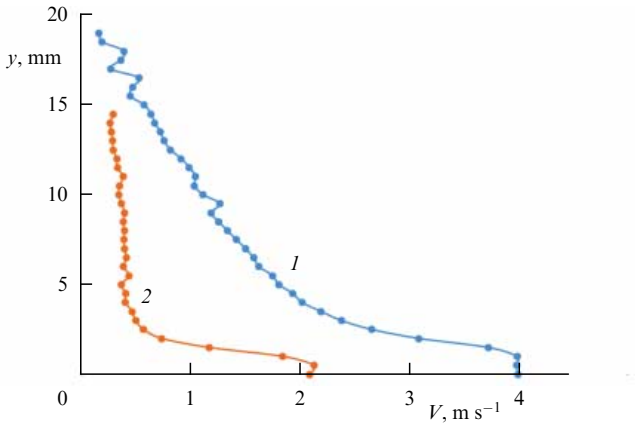

Figure 17. Vertical profiles of induced velocity $V(y)$ downstream from the last discharge gap at the pulse frequency of 12 kHz and voltage amplitude of 4.8 kV for model I (*1*) and model II (*2*).

comparative analysis makes the most sense for the coincident power supply conditions and the parameters close to the ultimate permissible values.

The experimental dependence of the induced flow maximum velocity V on the power P consumed by the actuators for various values of frequency f and voltage amplitude U_m is shown in Fig. 15, where the first values (in the rectangles) are the frequency f [kHz], and the second ones are the values of U_m [kV]. The voltage in the experiment had a sawtooth form, with a linear growth and sharp drop, periodically deviating from zero to one side or the other. The total voltage sweep extended over $2U_m$ for this reason. From the given dependence, it can be seen that V increases first, and then saturates. Some studies mention that the velocity can decrease for high values of voltage and frequency of the actuator power supply, because of reduced homogeneity in the barrier discharge glow [16]. In our case, the saturation effect was evident in model I, which had a higher self-capacitance and, hence, higher energy consumption, given the supplied power of 300 W at the frequency of 12 kHz and the sawtooth voltage amplitude of 4.8 kV.

The analysis of data obtained showed a linear increase in the temperature of the actuator plate with increasing the supplied power. For the frequency of 12 kHz and sawtooth voltage amplitude of 4.8 kV, the temperature rose to 100 °C, which is already close to the critical value. For this reason, the parameters mentioned were taken as basic ones in comparing both models of multidischarge plasma actuators.

The measurement results for the longitudinal velocity induced in air at the height $y = 0.5$ mm from the model surface for an optimal pulse amplitude up to 4.8 kV, the discharge frequency of 12 kHz, the mean power supply up to 300 W, and the maximum admissible surface temperature of 100 °C for the models of multidischarge actuator systems explored here are presented in Fig. 16. It demonstrates that for model II with the classic electrode system the velocity periodically drops to almost zero, which is related to the excitation of oppositely directed air flows near the surface. At the same time, model I maintains a practically uniform air flow with a substantially higher velocity.

The vertical velocity profiles in Fig. 17, measured downstream of the last discharge gap in the section corresponding to the maximum of the longitudinal velocity, indicate that, in addition to increased velocity, model I also maintains an air flow extending higher from the plate surface.

The main characteristics defining the efficiency of multidischarge actuator systems are the space and time mean horizontal bulk force exerted by them on the gas over an actuator and mean electric power consumed. Based on these characteristics, computed using the technique described in Ref. [65], one may estimate for the systems considered the energy efficiency coefficient C_{eff} of a single actuator, which is defined as the ratio of mean integral bulk force F_1 generated by a single actuator to the mean consumed power P_1 computed per unit length of the outer electrode: $C_{eff} = F_1/P_1$.

To estimate the mean force, which is the algebraic sum of positive bulk Coulomb force and negative surface friction force, a variant of the integral momentum approach was invoked [71].

To confirm that the measurement data are reliable, the power consumed by actuators was estimated by the methods of volt–coulomb [66] and volt–ampere [65] characteristics, which showed close agreement in their results.

Table 4 presents estimates of maximum values for F_1, W_1, and C_{eff} for the multidischarge actuator systems studied here [72, 73].

Table 4. Maximum values of mean integral bulk force F_1, mean consumed power P_1, and energy efficiency C_{eff} of a single actuator for the explored models of multidischarge actuator systems.

Model	F_1, mN m^{-1}	P_1, W m^{-1}	$C_{\text{eff}} \times 10^4$, s m^{-1}
I	4	45	0.9
II	1.4	65	0.2

The values achieved indicate that the multidischarge actuator system designed by us for active control of gas flows in boundary layers on extended aerodynamic surfaces have the basic parameters of induced air flow and the values of energy efficiency and bulk force acting on the flow that are substantially higher than in their analogs worldwide.

We should mention that we are presently carrying out research aimed at the development of the promising system of flying apparatuses with an EHD driver. An apparatus providing the lift force through the generation of an EHD flow came to be known as ionocraft. Such an apparatus has no moving parts, and its working medium is the ambient atmosphere, so that only electric energy is transferred to kinetic energy. Now, based on efficient multidischarge actuator systems, we succeeded in passing an important step by creating an ionocraft capable of lifting its weight, including its own power supply system.

6. Conclusions

Thus, we proposed and explored a new approach to the generation of strong EHD flows forming when gas discharge plasma interacts with the ambient gaseous medium, based on utilizing a powerful ion source provided by barrier discharge extended over a dielectric surface.

We also proposed a theoretical model of electrodynamic flow maintained by a high-frequency barrier discharge, which considers a beam of charged particles propagating through a gaseous medium in an external electric field and describes the process of gas flow acceleration under the action of a pressure gradient of electric forces caused by the motion of an ion spatial charge in the external electric field.

A model has been developed to compute ultimate characteristics of EHD flow, which allows applying simplified analytical expressions for quantitative estimates of volt–ampere and velocity dependences of the air flow. Computer simulations of EHD flow have been performed for a planar-cylindrical electrode module consisting of a plasma ion emitter made of a dielectric tube and an ion collector made of a flat metal grid. Their results agree well with available experimental data.

Electric discharge systems have been developed for active control of flows with a high volumetric gas flow rate. In atmospheric air, a flow velocity of 2 m s^{-1} has been achieved over an area of 80 cm^2. The volumetric flow rate in this case is more than 15 l s^{-1}, which is comparable to gas flows maintained by electromechanical fans.

The possibility has been explored of actively controling gas flows with the aid of the EHD process, aimed at reducing surface friction on aerodynamic surfaces and, hence, reducing power consumption and atmospheric pollution. A multidischarge actuator system has been created to generate a continuous, unidirectional air flow in boundary layers over extended aerodynamical surfaces, characterized by a higher energy efficiency and bulk force action on a fast flow than its analogs worldwide.

References

1. Hauksbee F *Physico-mechanical Experiments on Various Subjects* (London: R. Brugis, 1709) p. 46
2. Peek F W (Jr.) *Dielectric Phenomena in High-Voltage Engineering* (New York: McGraw-Hill, 1929)
3. Robinson M *AIEE Trans.* **80** 143 (1961)
4. Leonard G L, Mitchner M, Self S A *J. Fluid Mech.* **127** 123 (1983)
5. Owsenek B, Seyed-Yagoobi J *J. Heat Transfer* **119** 604 (1997)
6. Madhan R C M, Roth J R, Sin H, in *41st Aerospace Sciences Meeting and Exhibit 6 – 9 January 2003, Reno, Nevada* (Reston, VA: American Institute of Aeronautics and Astronautics, 2003) p. 531
7. Kaptsov N A *Koronnyi Razryad i Ego Primenenie v Elektrofil'trakh* (Corona Discharge and Its Applications in Electric Filters) (Moscow: Gostekhizdat, 1947)
8. Vereshchagin I P *Koronnyi Razryad v Apparatakh Electron-ionnoi Tekhnologii* (Corona Discharge in Apparatuses of Electron–Ion Technology) (Moscow: Energoatomizdat, 1985)
9. Mclean K J *IEEE Proc. Sci. Measur. Technol.* **135** 347 (1998)
10. Brown D L et al., in *Proc. of the XIIIth Intern. Symp. on High Voltage Engineering, Delft, Netherlands, 25 – 29 August, 2003* (Delft, Nederland, 2003)
11. Yue Y et al. *Plasma Sci. Technol.* **8** 697 (2006)
12. Go D B et al. *J. Appl. Phys.* **102** 053302 (2007)
13. Honer K A et al. *Thermal News* **11** 1 (2008)
14. El-Khabiry S, Colver G M *Phys. Fluids* **9** 587 (1997)
15. Leger L, Moreau E, Touchard G *IEEE Trans. Industry Appl.* **38** 1478 (2002)
16. Reece Roth J *Phys. Plasmas* **10** 2117 (2003)
17. Reece Roth J, Xin D, in *44th Aerospace Sciences Meeting and Exhibit, Reno, Nevada, 9 – 12 January 2006*
18. Gorkin S B, Kozlov B A, Solov'ev V I *Izv. Ross. Akad. Nauk Ser. Fiz.* **58** (2) 42 (1994)
19. Shuaibov A K *Tech. Phys.* **43** 1083 (1998); *Zh. Tekh. Fiz.* **68** (9) 84 (1998)
20. Treshchalov A, Lissovski A, Chikeev E *Proc. SPIE* **4747** 253 (2002)
21. Khomich V Yu, Yamshchikov V A "Formirovanie elektricheskogo vetra s pomoshch'yu vysokochastotnogo bar'ernogo razryada" ("Formation of electric wind with the help of high-frequency barrier discharge"), Preprint TsNP IPEF RAN (Moscow: Lebedev Physics Institute, 2003)
22. Kozlov B A, Solov'ev V I *Tech. Phys.* **52** 892 (2007); *Zh. Tekh. Fiz.* **77** (7) 70 (2007)
23. Moshkunov S I et al. *Quantum Electron.* **41** 1093 (2011); *Kvantovaya Elektron.* **41** 1093 (2011)
24. Chizhevsky A L *Aeroionifikatsiya v Narodnom Khozyaistve* (Aeroionification in National Economy) (Moscow: Gosplanizdat, 1960)
25. Kozlov B A, Solov'ev V I *Tech. Phys.* **51** 821 (2006); *Zh. Tekh. Fiz.* **76** (7) 1 (2006)
26. Nebogatkin S V et al., in *XLIII Mezhdunar. Zvenigorodskaya Konf. po Fizike Plazmy i Upravlyaemomu Termoyadernomu Sintezu, 8–12 Fevralya 2016 g., Zvenigorod. Sbornik Tezisov Dokladov* (XLIII Intern. Zvenigorod Conf. on Plasma Physics and Controlled Fusion, 8–12 February 2016, Zvenigorod. Collection of Talk Abstracts) (Eds L M Kovrizhnykh et al.) (Moscow: PLAZMAIOFAN, 2016)
27. Nebogatkin S V et al. *Prikl. Fiz.* (4) 111 (2009)
28. Apollonov V V et al. *Sov. J. Quantum Electron.* **15** 1 (1985); *Kvantovaya Elektron.* **12** 5 (1985)
29. Khomich V Yu, Yamshchikov V A *Osnovy Sozdaniya Sistem Elektrorazryadnogo Vozbuzhdeniya Moshchnykh CO_2-, N_2- i F_2-Lazerov* (Fundamentals of Electric Discharge Excitation Systems Design for Powerful CO_2, N_2 and F_2 Lasers) (Moscow: Fizmatlit, 2014)
30. Mikolutskii S I et al. "Moshchnyi istochnik elektricheskogo vetra na osnove vysokochastotnogo bar'ernogo razryada v gaze" ("Powerful electric wind source on the basis of high-frequency barrier discharge in gas"), Preprint (Moscow: IEE RAN, 2009)
31. Moshkunov S I et al. *Prikl. Fiz.* (6) 32 (2011)
32. Kasayapanand N, Kiatsiriroat T *Energy* **32** 1343 (2007)
33. Karpov S V, Krichtafovitch I A, in *Proc. of the COMSOL Multiphysics User's Conf., Boston, 2005*

34. Jayanty V et al., in *Proc. of the ESA Annual Meeting on Electrostatics, June 17 – 19, 2008, Minneapolis, MN*
35. Yavorsky B, Detlaf A *Handbook of Physics* (Moscow: Mir, 1972); Translated from Russian: *Spravochnik po Fizike* (Moscow: Nauka, 1964)
36. Kuleshov P S *Electron. J.* "*Issledovano v Rossii*" **8** 2336 (2005)
37. Kikoin I K (Ed.) *Tablitsy Fizicheskikh Velichin* (Tables of Physical Quantities) (Moscow: Atomizdat, 1976)
38. Arishev Yu S et al. *Plasma Phys. Rep.* **26** 157 (2000); *Fiz. Plazmy* **26** 172 (2000)
39. Ivanov E V et al. *Prikl. Fiz.* (2) 122 (2006)
40. Ivanov E V, Moshkunov S I, Khomich V Yu *Instrum. Exp. Tech.* **49** 80 (2006); *Prib. Tekh. Eksp.* (1) 88 (2006)
41. Zheleznov Yu A, Khomich V Yu *Tech. Phys. Lett.* **32** 136 (2006); *Pis'ma Zh. Tekh. Fiz.* **32** (3) 90 (2006)
42. Moshkunov S I et al. *Quantum Electron.* **41** 366 (2011); *Kvantovaya Elektron.* **41** 366 (2011)
43. Malashin M V et al. *Instrum. Exp. Tech.* **57** 140 (2014); *Prib. Tekh. Eksp.* (2) 53 (2014)
44. Khomich V Yu et al. *IEEE Trans. Plasma Sci.* **42** 3314 (2014)
45. Malashin M V, Moshkunov S I, Khomich V Yu *Instrum. Exp. Tech.* **59** 222 (2016); *Prib. Tekh. Eksp.* (2) 71 (2016)
46. Nebogatkin S V et al. *Usp. Prikl. Fiz.* **2** 595 (2014)
47. Rebrov I E, Khomich V Yu, Yamshchikov V A *J. Phys. Conf. Ser.* **652** 1 (2015)
48. Rebrov I E et al., in *The 23th Annual Intern. Conf. on Advanced Laser Technologies ALT'15, Faro, Portugal, September 7 – 11, 2015. Book of Abstracts* (2015) p. 175
49. Rebrov I E, Khomich V Yu, Yamshchikov V A, in *Sovremennye Problemy Fiziki Plazmy i Fizicheskoi Elektroniki. Materialy II Vseross. Konf., 25–28 Noyabrya 2015 g.* (Current Problems in Plasma Physics and Physical Electronics. Materials of II All-Russia Conf., 25–28 November, 2015) (Ed. A F Aleksandrov) (Makhachkala: Izd. DGU, 2015) p. 122
50. Rebrov I E, Khomich V Yu, Yamshchikov V A, in *12th Intern. Conf. on Gas Discharge Plasmas and Their Applications, GDP 2015, September 6 – 11, 2015, Tomsk, Russia* (2015) p. 202
51. Rebrov I E, Khomich V Yu, Yamshchikov V A *J. Phys. Conf. Ser.* **652** 012036 (2015)
52. Rebrov I E, Khomich V Yu, Yamshchikov V A, in *XLIII Mezhdunar. Zvenigorodskaya Konf. po Fizike Plazmy i Upravlyaemomu Termoyadernomu Sintezu, 8–12 Fevralya 2016 g., Zvenigorod. Sbornik Tezisov Dokladov* (XLIII Intern. Zvenigorod Conf. on Plasma Physics and Controlled Fusion, 8–12 February 2016, Zvenigorod. Collection of Talk Abstracts) (Ed. L M Kovrizhnykh et al.) (Moscow: PLAZMAIOFAN, 2016)
53. Baranov V Yu et al. *Sov. Phys. JETP* **52** 240 (1980); *Zh. Eksp. Teor. Fiz.* **79** 478 (1980)
54. Vartapetov S K et al. *Quantum Electron.* **39** 714 (2009); *Kvantovaya Elektron.* **39** 714 (2009)
55. Moshkunov S I et al. *Plasma Phys. Rep.* **38** 1040 (2012); Translated from Russian: *Prikl. Fiz.* (6) 32 (2011)
56. Moreau E *J. Phys. D* **40** 605 (2007)
57. Roth J R, Sherman D M, Wilkinson S P *AIAA J.* **38** 1166 (2000)
58. Benard N, Moreau E *Exp. Fluids* **55** (11) 1 (2014)
59. Do H et al. *Appl. Phys. Lett.* **92** 071504 (2008)
60. Benard N et al. *Proc. of the Electrostatic Joint Conf., June 16 – 18, 2009, Boston, MA, USA*
61. Berendt A, Podliński J, Mizeraczyk J *Eur. Phys. J. Appl. Phys.* **55** 13804 (2011)
62. Debien A, Benard N, Moreau E *J. Phys. D* **45** 215201 (2012)
63. Hao J et al. *Sci. China Phys. Mech. Astron.* **57** 345 (2014)
64. Kuryachii A P et al. *Uchenye Zapiski TsAGI* **44** (3) 3 (2013)
65. Gamirullin M D et al. *Uchenye Zapiski TsAGI* **45** (6) 28 (2014)
66. Gamirullin M D et al. *Prikl. Fiz.* (5) 95 (2015)
67. Manley T C *Trans. Electrochem. Soc.* **84** 83 (1943)
68. Kriegseis J, Grundmann S, Tropea C *J. Appl. Phys.* **110** 013305 (2011)
69. Ashpis D, Laun M, Griebeler E, in *50th AIAA Aerospace Sciences Meeting Including the New Horizons Forum and Aerospace Exposition, 9 – 12 January 2012, Nashville, Tennessee*, AIAA 2012-0823, https://dx.doi.org/10.2514/6.2012-823
70. Jiang H et al. *Dielectrics Electrical Insulation* **20** 4 (2013)
71. Kriegseis J et al., in *50th AIAA Aerospace Sciences Meeting Including the New Horizons Forum and Aerospace Exposition, 9 – 12 January 2012, Nashville, Tennessee*, AIAA 2012-0411, https://dx.doi.org/10.2514/6.2012-411
72. Aleshin B S, Khomich V Yu, Chernyshev S L *Dokl. Phys.* **61** 601 (2016); *Dokl. Ross. Akad. Nauk* **471** 662 (2016)
73. Chernyshev S L et al. *Aerospace Sci. Technol.* **59** 155 (2016)